

Anomalous Scaling in Shell Model Turbulence

James Creswell,¹ Viatcheslav Mukhanov,¹ and Yaron Oz²

¹Ludwig Maximilian University, Theresienstr. 37, 80333 Munich, Germany

²School of Physics and Astronomy, Tel-Aviv University, Tel-Aviv 69978, Israel

(Dated: February 13, 2024)

Shell model turbulence is a simplified mathematical framework that captures essential features of incompressible fluid turbulence such as the energy cascade, intermittency and anomalous scaling of the fluid observables. We perform a precision analysis of shell model of a complex velocity field in the steady state turbulent regime, including a calculation of the leading hundred anomalous scaling exponents, the probability distribution function of the magnitude and phase of the velocity and the correlations among them at different shells. We analyze the tail of velocity distribution function and find that the high moments exhibit a linear scaling that differs from Kolomogorov's. We explain the origin of this asymptotic scaling that offers a new insight to the structure of fluid turbulence.

I. INTRODUCTION

Turbulence is an ubiquitous irregular motion of fluid, such as air or water, that exhibits rapid and unpredictable changes in velocity, pressure, and density within the fluid. Turbulence is inherently difficult to predict and model accurately due to its complex, non-linear nature at a wide range of scales, from large eddies down to very small ones, making it challenging to analyze analytically [1]. A captivating facet of turbulence is the anomalous scaling of fluid observables at the inertial range of scales, and their deviation from Kolmogorov linear scaling [2] due to intermittency. These exponents hold the key to unraveling the statistical intricacies and structural complexities of turbulent flows. Analytical derivations of scaling exponents are rare [3]. A significant challenge arises in accurately measuring these scaling exponents. Despite compelling experimental and numerical evidence showcasing deviations from Kolmogorov scaling, the precision of available data remains insufficient [4] to definitively differentiate among the various proposed models in the real world three-dimensional turbulence [5–8]. Hence, the pursuit of precision turbulence emerges as an imperative paradigm shift in turbulence research.

Shell models provide a simplified mathematical framework to study fluid turbulence [9–11], and they capture some of the essential features of turbulence, while reducing the complexity of the equations involved. This framework can be particularly useful to model the energy cascade, intermittency and the statistical properties of turbulent fluid flows. Compared to solving the Navier-Stokes equations, which are computationally expensive, shell models are computationally efficient, making them natural playgrounds for developing precision turbulence. Numerical calculations of scaling exponent in shell models have been carried out for the low moments of the velocity probability distribution function in [11–15]. A hidden symmetry in shell models has been proposed in [16].

The aim of this letter is to address precision turbulence in the framework of the complex velocity shell model introduced in [11]. We will perform a detailed analysis of shell model of the complex velocity field in the steady

state turbulent regime, including a calculation of the leading hundred anomalous scaling exponents, the probability distribution function of the velocity field magnitude and its phase and the correlations among the velocities at different shells. We will analyze the tail of velocity distribution function and show that the high moments of the distribution exhibit a linear scaling that differs from Kolmogorov's. We will uncover the origin of this asymptotic linear scaling and offer a new insight to the structure of fluid turbulence.

The letter is organized as follows. In section II we briefly review the SABRA shell model for a complex velocity field, present the anomalous scaling exponents ζ_p up to $p = 100$ and discuss the large p asymptotics. In section III we consider the joint probability distribution function of the the velocities at different shells including the magnitude and phase marginal distributions and their correlation structure. Section IV is devoted to a discussion. Details of the calculations and additional plots are given in the Supplemental Materials.

II. TURBULENCE SCALING IN SHELL MODEL

A. SABRA model

We will consider the SABRA shell model [11]. It consists of complex valued shells velocity scale field indexed by the shell number, u_n , evolving in time according to:

$$\frac{du_n}{dt} = i \left(ak_{n+1}u_{n+2}u_{n+1}^* + bk_nu_{n+1}u_{n-1}^* - ck_{n-1}u_{n-1}u_{n-2} \right) - \nu k_n^2 u_n + f_n, \quad (1)$$

where $n = 1, 2, \dots$ indexes the shells. a , b , and c are real-valued constants, k_n are wavenumbers obeying $k_n = k_0 \lambda^n$ for some constants k_0 and λ , and ν is a viscosity parameter. f_n describes an external forcing, taken to be Gaussian random noise, which will be applied to the first shells (IR). Energy conservation dictates that $a + b + c = 0$. The shell model reaches a steady state and exhibits anomalous scaling at the inertial range of scale $n_f \ll n \ll n_\nu$ where n_f and n_ν correspond to the forcing

scale in the IR and the viscous scale in the UV. One searches for a scaling

$$\langle |u_n|^p \rangle \propto k_n^{-\zeta_p}, \quad (2)$$

where the average is taken over the space of solutions in the steady state turbulent regime. The scaling exponents ζ_p are believed to be universal and independent of the force and viscous structures. Our main goal is to determine accurately these scaling exponents up to $p = 100$, using simulations in which equation (A1) is solved numerically.

Our choice of parameters and forcing follows [11]: $a = 1, b = c = -0.5, \lambda = 2, k_0 = 2^{-4}, \nu = 4 \times 10^{-11}$. We will have a total of 50 shells, although not all will be part of the data analysis of the inertial range. The forcing term f_n is applied to the first two shells (see details in the Supplementary Materials). Although the details of the forcing are not expected to change the results we are seeking, to be explicit we are using the same type of coloured (correlated) Gaussian random noise described in [11]. For the initial condition, the energy is divided between the first two shells randomly:

$$u_1 = \sqrt{\alpha E_0} e^{2\pi i \beta}, u_2 = \sqrt{(1-\alpha) E_0} e^{2\pi i \gamma}, \quad (3)$$

An initial energy $E_0 = 10$ is chosen, and α, β, γ are drawn uniformly from the unit interval. For completeness, we check the robustness of the calculated scaling exponents for different values of E_0 and ν , as well as different procedures for generating the forcing including correlated noise and white noise. Further information is available in the Supplementary Materials.

B. Scaling Exponents

A universal structure of turbulence is expected only at the inertial range of scales $n_f \ll n \ll n_\nu$. In order to determine this range we use the analytical result for the third moment $\zeta_3 = 1$ which serves as a reference point to evaluate the numerical the simulations. The departure of ζ_3 from 1 at a given accuracy gives the breakdown of the inertial range to that accuracy. This is shown in the Supplementary Materials.

In Table I we list the moments scaling exponents up to hundred and we plot them in Fig. 2. The low moments agree with the results of [11]. The fit to Eq. (A1) is performed using least-squares regression. The errors are calculated as

$$\text{std}(\zeta_p) = \frac{\text{best-fit residual}}{\text{degrees of freedom}} \times C,$$

where C is the component of the covariance matrix corresponding to the parameter ζ_p . This quantifies the statistical error of the fit.

p	ζ_p	p	ζ_p
1	0.402 ± 0.004	23	5.442 ± 0.340
2	0.730 ± 0.008	24	5.660 ± 0.358
3	1.002 ± 0.012	25	5.877 ± 0.375
4	1.272 ± 0.019	26	6.095 ± 0.393
5	1.513 ± 0.031	27	6.313 ± 0.410
6	1.744 ± 0.048	28	6.530 ± 0.428
7	1.968 ± 0.065	29	6.748 ± 0.446
8	2.188 ± 0.082	30	6.966 ± 0.463
9	2.407 ± 0.098	35	7.757 ± 0.551
10	2.624 ± 0.114	40	8.838 ± 0.638
11	2.841 ± 0.129	45	9.921 ± 0.724
12	3.057 ± 0.144	50	11.004 ± 0.811
13	3.273 ± 0.159	55	12.088 ± 0.897
14	3.490 ± 0.178	60	13.172 ± 0.983
15	3.706 ± 0.196	65	14.256 ± 1.069
16	3.923 ± 0.214	70	15.341 ± 1.154
17	4.140 ± 0.232	75	16.426 ± 1.235
18	4.356 ± 0.250	80	17.511 ± 1.317
19	4.573 ± 0.269	85	18.597 ± 1.399
20	4.790 ± 0.286	90	19.683 ± 1.481
21	5.007 ± 0.304	95	20.768 ± 1.562
22	5.225 ± 0.322	100	21.854 ± 1.644

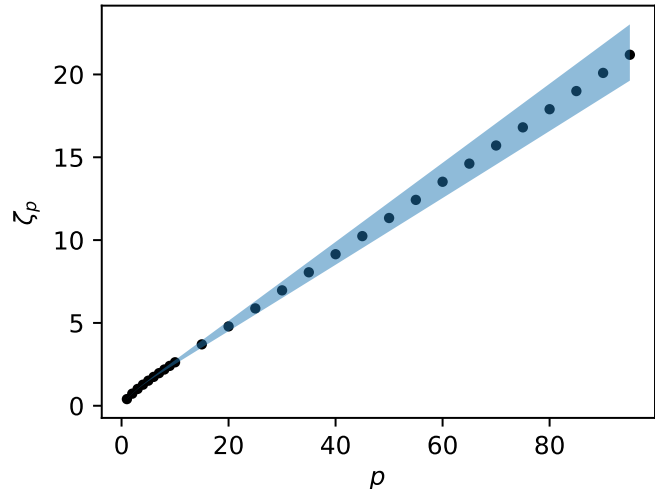


FIG. 1. Scaling exponents up to $p = 100$, with the 90% confidence region shown in blue. The uncertainty is the systematic error (see the appendix for discussion).

C. Large p Asymptotics

Fig. 2 indicates that the large p limit of the anomalous scaling exponents is $\zeta_p = \frac{p}{5}$, which is a linear scaling that differs from Kolmogorov's $\zeta_p = \frac{p}{3}$. In order to understand the origin of this asymptotic scaling consider the marginal probability distribution functions (PDFs) of $|u_n|$, $f(|u_n|)$. The main contribution to the higher moments comes from the maximal value $|u_n| = |u_{max}|$. More precisely, the PDFs $|u_n|^p f(|u_n|)$ at large p have a sharp peak at $|u_n| \sim \alpha k_n^{-\frac{1}{5}} = \alpha 2^{-\frac{p}{5}}$, where α is a constant which is independent of p , see Fig. 2, and Fig. 3

where we plot the maximal $|u_n|$ in each shell.

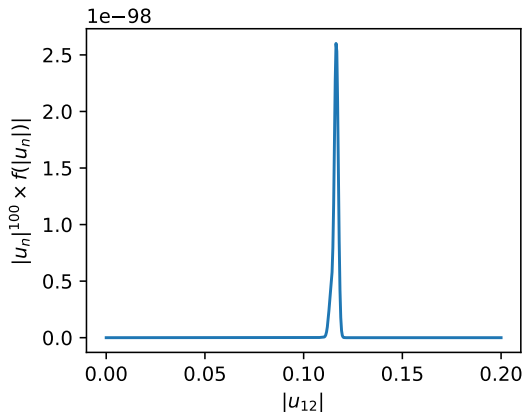


FIG. 2. Moment distribution function, $|u_n|^p \times f(|u_n|)$, for $p = 100$, where $f(|u_n|)$ is the PDF of the velocity magnitude. The 12th shell ($n = 12$) is plotted.

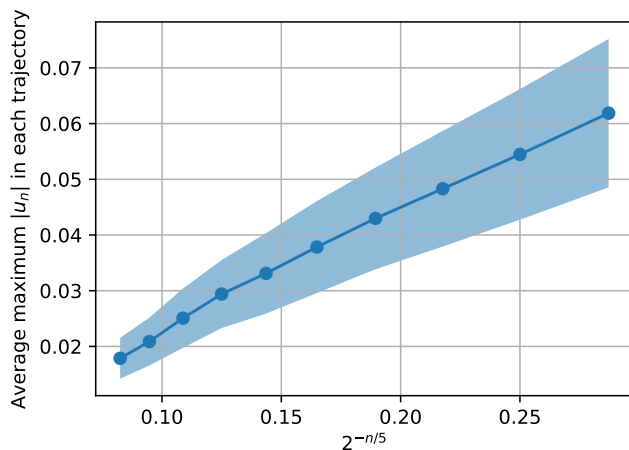


FIG. 3. Maximal velocity magnitude $|u_n|$ in each shell versus $k_n^{-1/5} = 2^{-n/5}$ where n is the shell number. We see a linear scaling.

This reveals an interesting structure of turbulence scaling and leads us to propose that

$$\lim_{p \rightarrow \infty} (|u_n|^p f(|u_n|)) = \delta(|u_n| - \alpha k_n^{-1/5}), \quad (4)$$

where α is a non-universal constant.

III. VELOCITY DISTRIBUTION FUNCTION

In the Supplemental Materials we plot the marginal probability distributions functions of the velocity magnitude $|u_n|$ and its phase. The magnitude PDFs can be approximated by a log-normal distribution for small velocities with the skewness increasing with n . However,

the log-normal distribution does not capture correctly the fast drop of the distribution at higher velocity magnitudes and its tail. The marginal phase PDFs are uniform, as expected [11].

A. Covariance matrix

The covariance matrices of velocity magnitudes and phases in different shells are shown in Fig. 4. In both cases the covariance is the normalized equal-time correlation function, i.e., the Pearson cross-correlation coefficient:

$$C(n, m) = \frac{\text{cov}(n, m)}{\sigma_n \sigma_m}, \quad (5)$$

where cov is the covariance estimated by multiplying equal times of two shells u_n and u_m , and σ_n and σ_m are the corresponding variances of each shell. The values of C range from -1 to 1 , where 1 means perfectly correlated. As seen in Fig. 4, there is a spreading of the off-diagonal velocity magnitude covariance $C(n, m)$ between two shells n and m as n and m increase. Putting the axes in logarithmic scales, the covariance matrix takes a uniform structure. The phase covariance matrix is diagonal, hence the phases at different shells are independent.

IV. DISCUSSION

We performed a precision analysis of shell model of a complex velocity field in the steady state turbulent regime and calculated the leading hundred anomalous scaling exponents, the probability distribution function of the velocity magnitude and its phase and the correlations among the velocities at different shells. We found that the high moments of the velocity magnitude PDF exhibit a linear scaling that differs from Kolomogorov's, whose origin is the dominant contribution from the maximum velocity. This provides an interesting new insight on the rare events of the turbulence in this model. Phenomenologically we found that a formula of the type [5]

$$f(p) = \frac{p}{5} + \frac{1}{2} \left(1 - (0.2)^{p/3} \right), \quad (6)$$

fits nicely the numerical data.

Note added While typing the manuscript we received [17], which contains some overlap with our calculation of the scaling exponents.

ACKNOWLEDGEMENTS

This work is supported in part by the Israeli Science Foundation Excellence Center, the US-Israel Binational Science Foundation, the Israel Ministry of Science and the LMU-TAU International Research Grant.

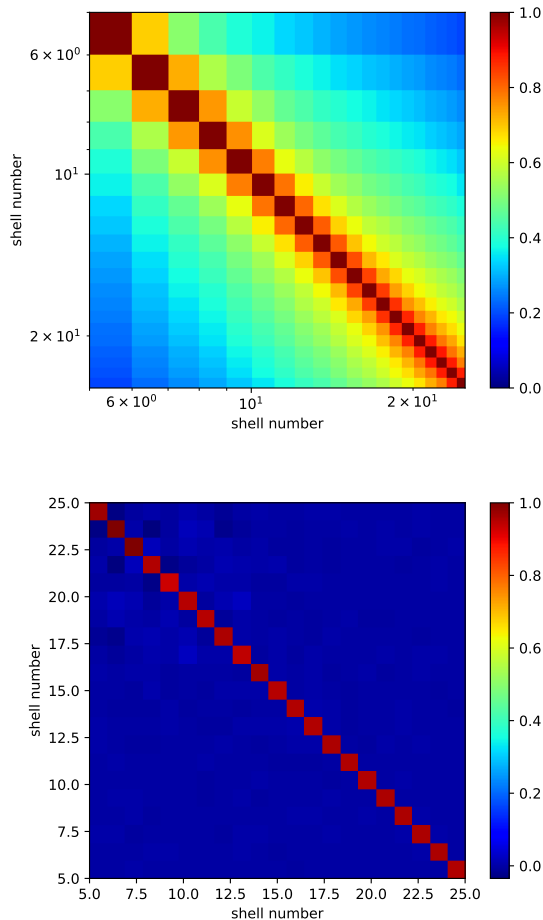


FIG. 4. Equal-time covariance of the velocity magnitude (upper plot) and phase (lower plot) between shells in the inertial range.

Further details and plots concerning the numerical analysis, correlation analysis, and other technical details are in the attached Supplementary Materials.

-
- [1] U. Frisch and A. N. Kolmogorov, *Turbulence: the legacy of AN Kolmogorov* (Cambridge university press, 1995).
- [2] A. Kolmogorov, The Local Structure of Turbulence in Incompressible Viscous Fluid for Very Large Reynolds' Numbers, *Akademiia Nauk SSSR Doklady* **30**, 301 (1941).
- [3] G. Falkovich, I. Fouxon, and Y. Oz, New relations for correlation functions in Navier-Stokes turbulence, *J. Fluid Mech.* **644**, 465 (2010), [arXiv:0909.3404 \[nlin.CD\]](https://arxiv.org/abs/0909.3404).
- [4] L. Biferale, F. Bonaccorso, M. Buzzicotti, and K. P. Iyer, Self-similar subgrid-scale models for inertial range turbulence and accurate measurements of intermittency, *Physical review letters* **123**, 014503 (2019).
- [5] Z.-S. She and E. Leveque, Universal scaling laws in fully developed turbulence, *Phys. Rev. Lett.* **72**, 336 (1994).
- [6] V. Yakhot, Mean-field approximation and a small parameter in turbulence theory, *Phys. Rev. E* **63**, 026307 (2001).
- [7] C. Eling and Y. Oz, The Anomalous Scaling Exponents of Turbulence in General Dimension from Random Geometry, *JHEP* **09**, 150, [arXiv:1502.03069 \[nlin.CD\]](https://arxiv.org/abs/1502.03069).
- [8] Y. Oz, Spontaneous symmetry breaking, conformal anomaly and incompressible fluid turbulence, *Journal of High Energy Physics* **2017**, 1 (2017).
- [9] E. B. Gledzer, System of hydrodynamic type admitting two quadratic integrals of motion, *Soviet Physics Doklady* **18**, 216 (1973).
- [10] K. Ohkitani and M. Yamada, Temporal Intermittency in the Energy Cascade Process and Local Lyapunov Analysis in Fully-Developed Model Turbulence, *Progress of Theoretical Physics* **81**, 329 (1989).
- [11] V. S. L'vov, E. Podivilov, A. Pomyalov, I. Procaccia, and D. Vandembroucq, Improved shell model of turbulence, *Phys. Rev. E* **58**, 1811 (1998).
- [12] L. Kadanoff, D. Lohse, J. Wang, and R. Benzi, Scaling and dissipation in the GOY shell model, *Physics of Fluids* **7**, 617 (1995), [arXiv:chao-dyn/9409001 \[nlin.CD\]](https://arxiv.org/abs/chao-dyn/9409001).
- [13] V. S. L'vov and I. Procaccia, Analytic calculation of the anomalous exponents in turbulence: Using the fusion rules to flush out a small parameter, *Phys. Rev. E* **62**,

- 8037 (2000).
- [14] R. Benzi, L. Biferale, M. Sbragaglia, and F. Toschi, Intermittency in turbulence: Computing the scaling exponents in shell models, [Phys. Rev. E](#) **68**, 046304 (2003).
 - [15] L. Biferale, Shell models of energy cascade in turbulence, [Annual Review of Fluid Mechanics](#) **35**, 441 (2003).
 - [16] A. A. Mailybaev, Shell model intermittency is the hidden self-similarity, [Phys. Rev. Fluids](#) **7**, 034604 (2022).
 - [17] X. M. de Wit, G. Ortali, A. Corbetta, A. A. Mailybaev, L. Biferale, and F. Toschi, Extreme statistics and extreme events in dynamical models of turbulence (2024), [arXiv:2402.02994 \[physics.flu-dyn\]](#).

Appendix A: Supplementary Materials

1. Simulation

In this section we describe the procedure for generating the simulated data. The equation (1),

$$\frac{du_n}{dt} = i(ak_{n+1}u_{n+2}u_{n+1}^* + bk_n u_{n+1}u_{n-1}^* - ck_{n-1}u_{n-1}u_{n-2}) - \nu k_n^2 u_n + f_n, \quad (\text{A1})$$

where $n = 1, 2, \dots$ indexes the shells, for the given parameters in use as described in the paper. Because the scale of u_n varies in different shells over multiple orders of magnitude, the system of differential equations becomes very stiff, i.e. numerical methods of integration are prone to instability and inaccuracy even with small step sizes. Implicit integration methods, in which previously computed data points are used to estimate the derivative at the current computation, improve the stability and robustness against stiffness. In particular, we choose a backward differentiation formula (BDF) method, with an adaptive order and adaptive time-step size, to perform the integration.

2. Noise

f_n describes an external forcing, taken to be Gaussian random noise, which is only applied to the first shells. Although the details of the forcing are not expected to change the results we are seeking, to be explicit we are using the same type of coloured (correlated) Gaussian random noise described in [1]. For the initial condition, a starting energy $E_0 = 10$ is chosen and divided between the first two shells randomly:

$$\begin{aligned} u_1(t=0) &= \sqrt{\alpha E_0} e^{2\pi i \beta}, \\ u_2(t=0) &= \sqrt{(1-\alpha)E_0} e^{2\pi i \gamma}, \end{aligned} \quad (\text{A2})$$

where α, β, γ are drawn uniformly from the unit interval. For the time evolution, f_n obeys:

$$\begin{aligned} f_n(t+dt) &= f_n(t)e^{-dt/\tau} + \\ &+ \sigma_n \sqrt{-2(1-e^{-2dt/\tau}) \log_{10}(\alpha)} e^{2\pi i \beta}, \end{aligned} \quad (\text{A3})$$

where dt is the timestep, τ is the forcing time-scale, $\tau \sim 1/(k_n u_n)$, and α and β are two uniform random numbers between 0 and 1 generated at each step. Following [1], we used $\sigma_1 = 5 \times 10^{-3}$ and $\sigma_2 = \sigma_1 \sqrt{-c/a}$.

In addition to the procedure for generating noise and initial conditions described above and used in the main simulations and analysis in the paper, we have also tried several different choices for the forcing and other parameters of the setup. This includes adjusting the viscosity ν , adjusting the initial energy E_0 , and different types of noise, including uncorrelated white noise ($\tau \rightarrow \infty$). In no case did these variations change the scaling exponents or other overall statistics. However, they did affect the time required to reach steady state.

3. Error analysis

There are two errors which apply to the calculation of the scaling exponents from finite data:

1. The uncertainty in the best-fit parameter of the slope.
2. The variation in the slope in finite segments of the data.

The first kind of error is being estimated using the standard least-squares error. The second kind of error is estimated using a procedure, in which the dataset is further subdivided into sections, and the fit performed on the partial datasets, which is quoted in Table I in the main paper.

Appendix B: Determination of the Inertial Range

The scaling power law is only expected within the inertial range of scale $n_f \ll n \ll n_\nu$ where n_f and n_ν correspond to the forcing scale in the IR and the viscous scale in the UV. For $p = 3$, an exact scaling $\zeta_p = 1$ can be derived analytically and this is used to determine the inertial range. The departure from $\zeta_p = 1$ at a given accuracy gives the breakdown of the inertial range to that accuracy. In Fig. 5 the spectrum for $p = 3$ and the range is zoomed around 1 to determine the inertial range. Adopting 1% as an accuracy threshold (corresponding to the red shaded region in 5), the simulations permit about 25 shells in the inertial range. In particular, shells 5 through 25 are retained for analysis below. In order to reach steady state, the data from $t = 0$ to $t = 500$ of each simulation is also excluded from the calculations of the scaling exponents in all analysis.

Appendix C: Large p Asymptotics

As the power p increases, the p th moment integrand, $|u_n|^p \times f(|u_n|)$, where f is the velocity magnitude probability distribution function, approaches to a narrow peak around the maximum velocity. This is illustrated in Fig. 6, where the moment integrand is plotted for $p = 25, 50, 75, 100$.

Appendix D: Marginal Distribution of Velocities Magnitudes and Phases

Complementary to the correlation analysis included in the paper, here we show the marginal distribution functions of the magnitude Fig. 7 and phases Fig. 8 of the complex-valued u_n trajectories.

Appendix E: Local Energy Dissipation

In Fig. 9 we plot the average local energy dissipation $k_n^2 |u_n|^2$ at each shell. We see a pick at the transition shells from the inertial range to the viscous regime. Restricting to the inertial range we get the expected scaling $k_n^2 |u_n|^2 \sim k_n^{2-\xi_2}$.

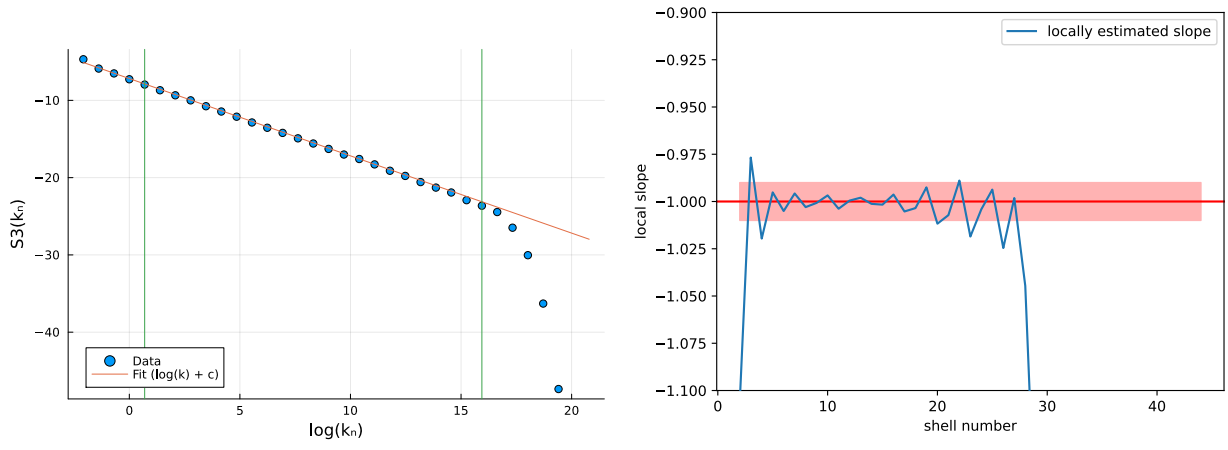


FIG. 5. Left: $S_3 = \langle |u_n|^3 \rangle$ spectrum. Right: Determination of the inertial range: ζ_3 within 1% of the analytically known result for $p = 3$.

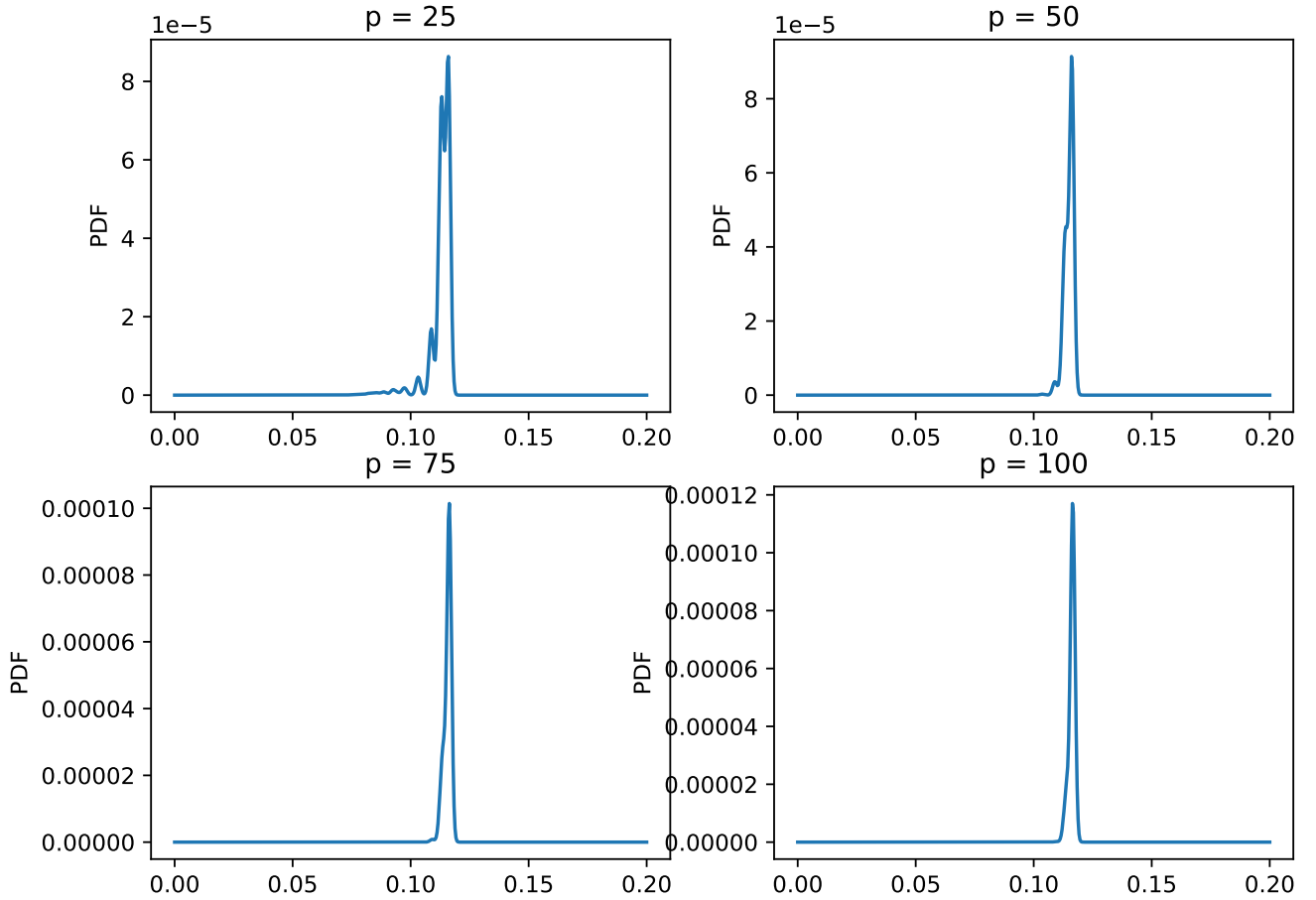


FIG. 6. As the power p increases, the p th moment integrand, $|u_n|^p \times f(|u_n|)$, where f is the distribution function, approaches to a narrow peak around the maximum velocity. In this figure the trend is shown for the 12th shell. The maximum velocity in this shell is 0.116.

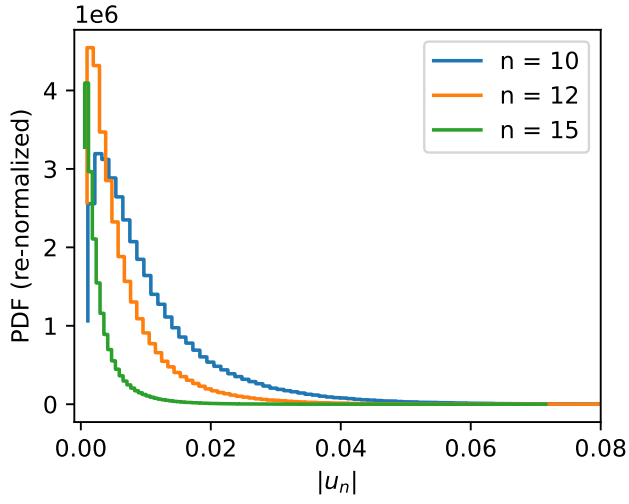


FIG. 7. Normalized marginal PDF of the velocity magnitude $|u_n|$ for the shells $n = 10, 12, 15$.

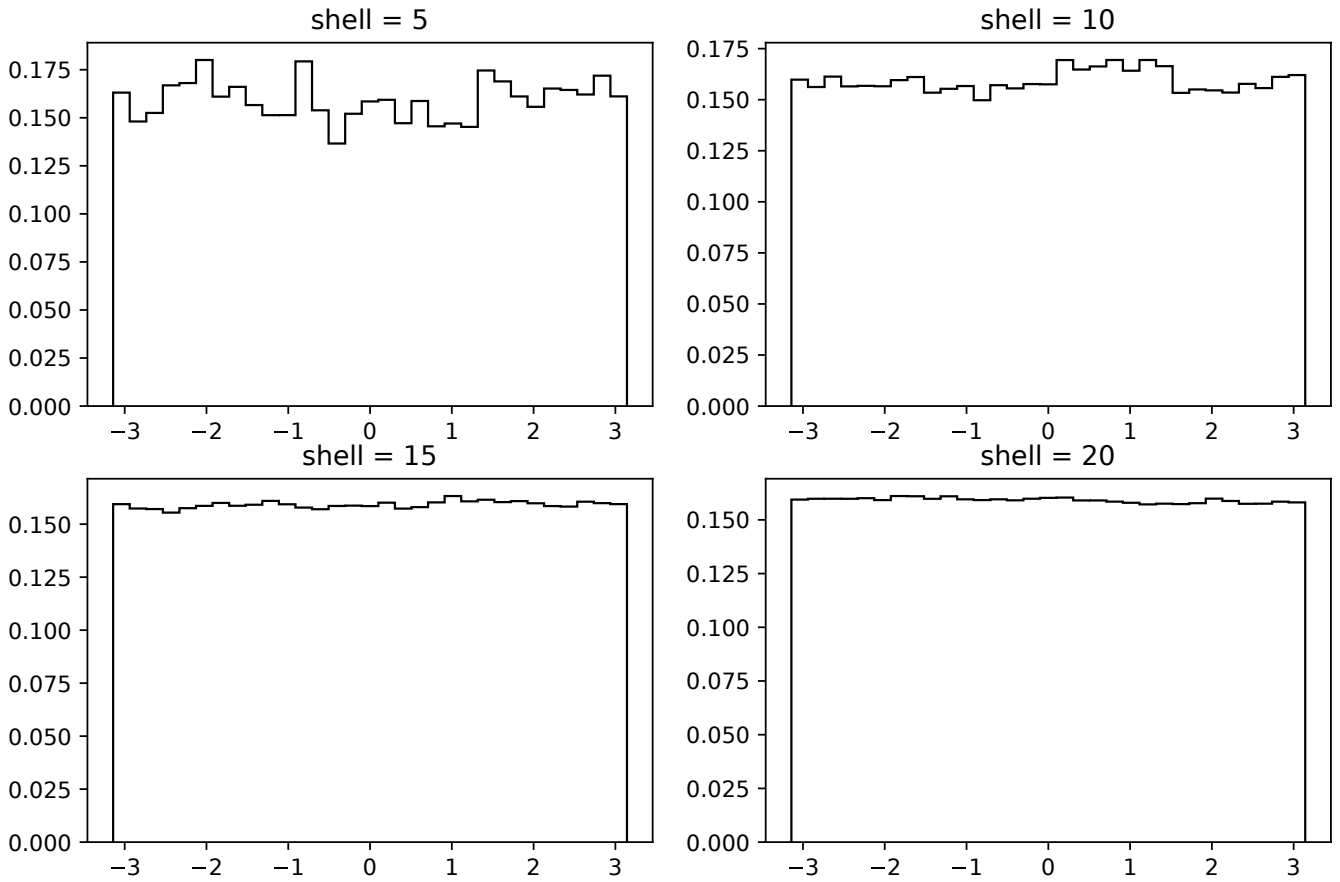


FIG. 8. Histograms of phases in each of several shells (marginals).

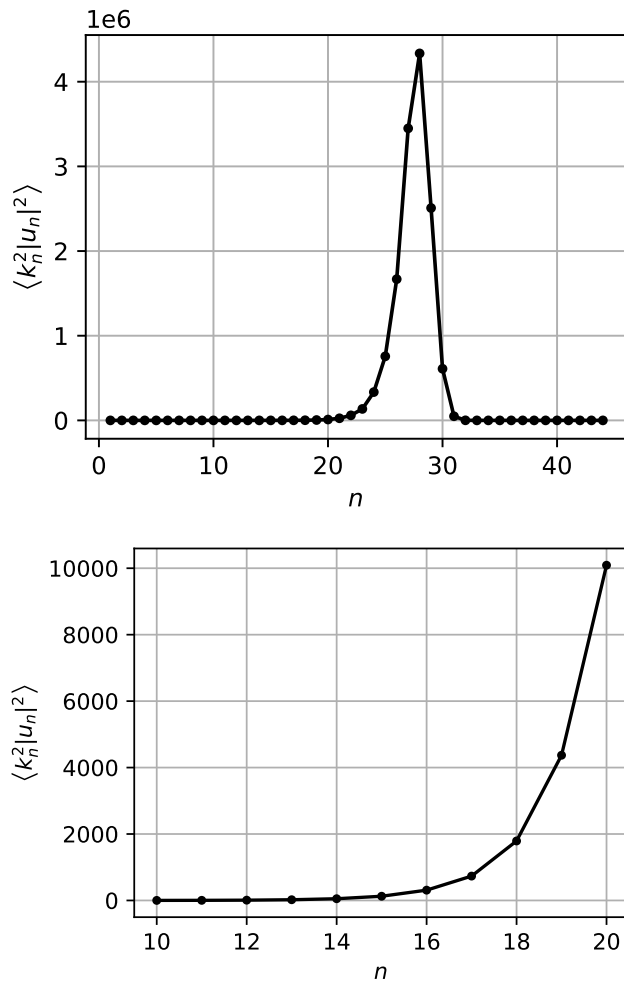


FIG. 9. The mean $k_n^2 |u_n|^2$ in each shell. Upper panel: the full range of shells. Lower panel: Zoom only on the shells of the inertial range.